Fuel 402 (2025) 136003

Contents lists available at ScienceDirect

Fuel

journal homepage: www.elsevier.com/locate/fuel

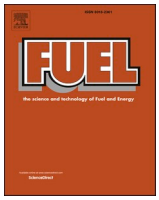

Full Length Article

Rapid post-combustion CO_2 capture by thermostatic concentration swing adsorption for amine-functionalized Al_2O_3

Shun Wang [a,b,c], Shujuan Wang [a,b], Yuqun Zhuo [a,b,c,*]

[a] Department of Energy and Power Engineering, Tsinghua University, Beijing 100084, PR China
[b] Key Laboratory of Thermal Science and Power Engineering of Ministry of Education, Tsinghua University, Beijing 100084, PR China
[c] Shanxi Research Institute for Clean Energy, Tsinghua University, Taiyuan 030000, PR China

ARTICLE INFO

Keywords:
Steam regeneration
Amine-functionalized Al_2O_3
Cycle process
Coal-fired power plants
Carbon capture

ABSTRACT

The increasing CO_2 leads to significant ecological changes, the control of CO_2 emissions has been a major concern worldwide. Amine-functionalized adsorbents have high CO_2 adsorption capacity under coal-fired power plants flue gas conditions. In this paper, a cycle process capable of rapid adsorption and desorption was found to be suitable for amine-functionalized adsorbents. The cycle process was conducted at constant 105 °C and a CO_2 adsorption capacity of 1.93 mmol/g was achieved only by changing the gas components (adsorption: 12.8 % CO_2, desorption: pure steam). The cycle process was validated to be more advantageous than the conventional TSA process in terms of energy cost and productivity. In the comparison with nitrogen as purge gas, it was observed that pure steam performed better with respect to CO_2 adsorption capacity, adsorption and desorption rates. Also, steam regeneration showed a different behavior: the temperature of the adsorbent rose when CO_2 was desorbed while reduced when CO_2 was adsorbed as the adsorption of water vapor released more heat. Considering the extremely high CO_2 emissions from coal-fired power plants, the rapid thermostatic concentration swing adsorption (TC-CSA), which eliminates the heating and cooling process, can greatly reduce the scale of carbon capture system and will be an attractive alternative cycle technology.

1. Introduction

As the main anthropogenic greenhouse gas [1], increasing carbon dioxide (CO_2) in the atmosphere is responsible for climate change [2–4]. In 2023, about 37.4 Gt CO_2 was emitted to the atmosphere [5]. Of all CO_2 sources, the power sector accounts for 36 %, greater than any other sector. Coal remains the largest single source of electricity worldwide, and by far the largest source of electricity sector emissions: it contributes just over one-third of electricity supply but is responsible for nearly three-quarters of electricity sector CO_2 emissions [6,7]. Therefore, decarbonization of power systems, especially coal-fired power plants, is of great importance for carbon reduction.

Solid adsorption are a promising carbon capture technology due to moderate adsorption heat, low toxicity and low equipment corrosivity compared to commonly employed amine-based solution [8]. It is categorized into physical and chemical adsorption based on the interaction forces. For physical solid adsorbents like zeolites [9], MOFs [10] and porous carbons, their adsorption capacity under flue gas conditions (50–60 °C, low CO_2 content of 10–15 vol%) is low. Also, the binding energy of the adsorbents with H_2O is higher than that with CO_2 because of the higher polarity of H_2O, thus leading to competitive adsorption between H_2O and CO_2 and more difficult desorption of H_2O. Amine-functionalized adsorbents have high adsorption capacity, selectivity and water resistance, and is regarded as a prospective carbon dioxide capture technology for coal-fired power plants flue gas [11–13].

Amine-functionalized adsorbents are mostly composed of amines and mesoporous or macroporous porous materials as support [14,15], and also include self-supporting amine adsorbents [16,17]. According to the binding mode of amines to porous media, there are three main classes of amine adsorbents [18]: class 1, amine-impregnated adsorbents, class 2, monolayer grafted adsorbents, and class 3, in situ polymerization. Amine-impregnated adsorbents are simple to prepare and can be obtained by stirring amines with porous materials in an organic solution such as methanol and evaporating to dryness. The impregnated amines can be categorized into polymer amines such as PEI [19,20] and low-molecular-weight amines such as TEPA,DETA,TETA [21,22]. The latter has a slightly higher adsorption capacity due to higher amine density, but is less thermally stable [23,24]. Both class 2 and 3 amine-

* Corresponding author at: Department of Energy and Power Engineering, Tsinghua University, Beijing 100084, PR China.
E-mail address: zhuoyq@tsinghua.edu.cn (Y. Zhuo).

https://doi.org/10.1016/j.fuel.2025.136003
Received 2 April 2025; Received in revised form 16 May 2025; Accepted 15 June 2025
Available online 21 June 2025

functionalized adsorbents were synthesized by grafting, aminosilanes containing methoxy or ethoxy groups are bonded to the –OH on the surface of supports, while for the class 3 adsorbents, the methoxy or ethoxy groups of aminosilanes are further hydrolyzed to form more –OH bonded to each other by controlling the amount of deionized water added in situ polymerization [25–27]. These adsorbents are more stable due to the presence of covalent bonds, but have a low CO_2 adsorption capacity due to lower amine density.

Different cycle processes should be applicated to amine-functionalized adsorbents to periodically adsorb and desorb CO_2, including PSA (Pressure swing adsorption) [28],VSA (Vacuum swing adsorption) [28,29], TSA(Temperature swing adsorption) [30,31] and the combination of the cycle process like VTSA(Vacuum temperature swing adsorption) [32,33], PVSA (Pressure swing adsorption) [34]. The principle of PSA and VSA is to change the partial pressure of CO_2 to achieve a difference in adsorption capacity. The processes seem to be attractive due to the low regeneration energy, always below 1.5 MJ/kg CO_2 [29,34]. However, it may not be advantageous considering the high quality of electricity used. And the low energy consumption was obtained by numerical simulation, which may differ a lot from actual capture conditions. For TSA process, adsorbents adsorb at a lower temperature while desorb at a higher temperature. The TSA process faces the problem of long heating and cooling time due to the low thermal conductivity of solid adsorbents. Some studies suggested to achieve rapid warming of the adsorbent bed by microwave [35] or electrical heating [36], but these methods also face the problem of high quality of electricity. When using TSA, purge gas needs to be considered. To avoid further mixing of CO_2 with the purge gas, one solution is to use pure CO_2 as the purge gas [37,38]. However, amine-functionalized adsorbents maintained high adsorption capacity at high temperatures and pure CO_2 gas streams. When the temperature exceeds 130 °C, the hydrothermal, thermal and chemical stability of the adsorbents face challenges [39,40].

Another suitable purge gas is steam because CO_2 and steam can be separated conveniently by cooling to room temperature [41,42]. Li [43] firstly introduced steam purge to the regeneration of amine-functionalized adsorbents in 2010, he also discovered that the CO_2 adsorption capacity 3-aminopropylsilyl-functionalized silica decreased by 20 % in just three cycles. Then it triggered many scholars to study the effect of water vapor on the stability of the amine-functionalized adsorbents [44–46]. Hammache [47] summarized five factors by which steam may affect amine-functionalized adsorbents: (1) the effect of the support, (2) a change in the nature of the amine, (3) a thermal effect, (4) a leaching of the amine by water, and (5) a change in the distribution of the amine on the support. Many studies have found that steam affected mostly on the support, so scholars focused on adjusting the support material to improve the hydrothermal stability. Min [48] observed that the thick-walled silica-based mesoporous MACS could improve the hydrothermal stability, amine-functionalized MACS only decreased by about 10 % when exposed to steam for 14 days, while SBA-15 decreased by 50 %. Compared to commonly used silica-based supports, alumina-supported amine adsorbents give better performance in terms of both capture capacity and amine efficiency [49]. Nonetheless Sakwa-Novak found that γ-alumina still converted to boehmite after more than 12 h of steam exposure, leading to a 60 % decrease in adsorption capacity. He also mentioned that short-term, multiple exposures affected less than long-term exposures. Unlike the general case where the steam regeneration occurs over 100 °C, Fujiki [50] combined steam regeneration with VSA process. The presence of pure steam at 40–60 °C enabled the use of steam purge at lower temperatures.

Considering the great CO_2 emission of about 8 t/min from a 600 MW coal-fired power plants, to reduce the carbon capture scale, the cycle time of the solid adsorbents is required to be as short as possible. Some studies have suggested that the cycle time is 15–30 min [42]. All the current cycle processes have adsorption and desorption conditions, and switching between these two conditions often takes a long time. Thermostatic concentration swing adsorption (TC-CSA) was proposed in this paper, which can realize adsorption and desorption process by only swapping the gas components. Compared to existing cycle strategies, TC-CSA has two main innovations: Compared to the commonly employed TSA, TC-CSA avoids the heating and cooling process, so the utilization efficiency of adsorbents is greatly improved; Although PSA and VSA also avoid the heating and cooling process, energy input is still needed to offset the CO_2 desorption heat and the temperature drop during desorption greatly reduces the desorption rate of solid amine adsorbents. While the temperature will increase during the desorption process in TC-CSA, thus increasing the desorption rate.

2. Materials and experimental methods

2.1. Preparation of PEI-γ- Al_2O_3

PEI-γ- Al_2O_3 was prepared as described in the literature [51]. 1 g γ-Al_2O_3 (Pore diameter: 20 nm, Purity: 99.99 %, Aladdin) was degassed at 100 °C for more than 3 h. 1 g PEI (Molecular weight Mw = 600, Purity: 99 %, Aladdin) was stirred in 30 mL methanol (Purity: 99.9 %, Concentration: 24.69 mol/L, Macklin) at room temperature for 30 min. Then the above solution was poured into the degassed γ-Al_2O_3 and stirred at 60 °C for 30 min in a 100 mL closed beaker. The beaker lid was then removed to vaporize the methanol and when the liquid was nearly evaporated, the residue was transferred to a vacuum oven and dried at 60 °C overnight. The final product is 50 % PEI-γ-Al_2O_3. The CO_2 adsorption capacity and amine loading of three batches of 50 % PEI-γ-Al_2O_3 were measured, as shown in Table 1. It can be found that these prepared adsorbents have good repeatability.

2.2. Measurement of cyclic CO_2 adsorption capacity

The CO_2 adsorption cycle unit is shown in Fig. 1. The CO_2 adsorption cycle experiment was performed as following: 1 g 50 % PEI-γ-Al_2O_3 was first placed in a cylindrical quartz adsorption column (Inner diameter: 13 mm, Height: 30 mm). Then, the furnace was turned on, after reaching a predetermined temperature, the adsorption/desorption occurs.

In the adsorption experiments, 14 SCCM premixed gas carried a certain amount of water vapor after passing through the water bubbler, and the oil bath temperature was fixed at 53 °C to control the water vapor content. The gas proportions of simulated flue gas were measured by gas chromatography (GC) and were: 12.9 % CO_2, 13 % H_2O and 74.1 % N_2. The CO_2 proportion of gas leaving the adsorption column was measured by GC. Then the CO_2 adsorption capacity q can be calculated by Equation (1) [52]. It was worth noting that there was a certain amount of dead volume from the adsorption column to GC, so a blank experiment was required to eliminate the effect before performing experiments. In the pre-experiment, the mass difference of the adsorption column was consistent with the adsorption capacity obtained by Equation (1), proving the accuracy of measurement results.

$$q = \int_0^t C_0(1 - C/C_0)\cdot V\cdot \mathrm{d}t/(22.4\cdot m) \quad (1)$$

where, C, C_0 represents the CO2 concentration at the outlet and inlet of the adsorption column, V is flow, SCCM. m is adsorbents mass.

In the desorption experiments, close the valves of the adsorption module, open the valves of the desorption module and turn on the syringe pump. 0.05 mL liquid water was completely vaporized by the

Table 1
CO_2 adsorption capacity and amine loading of three batches of 50% PEI-γ-Al_2O_3.

Batch	1	2	3
CO_2 adsorption capacity (mmol/g)	2.13	2.18	2.10
Amine loading (%)	49.39	49.67	50.37

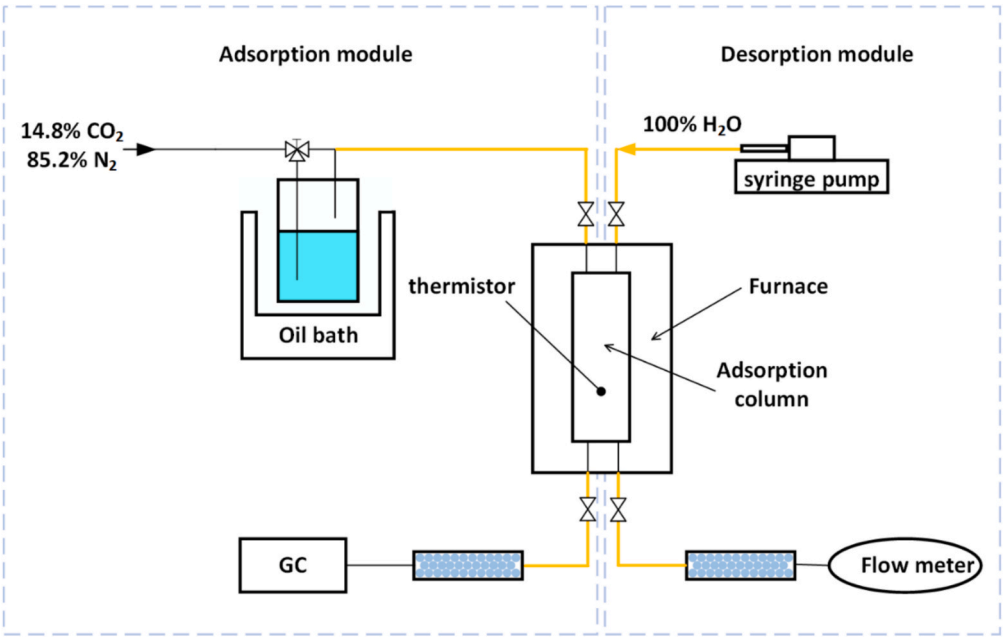

Fig. 1. CO_2 adsorption cycle unit. Orange lines represent heating lines.

heating line into the adsorption column. By periodically opening the valves of the adsorption and desorption modules, continuous cyclic adsorption experiments could be operated.

2.3. Characterization

N_2 physisorption was conducted on ASAP2460 at 77 K to estimate the pore structures of the supports and amine sorbents. Elemental analysis was conducted using Elementar vario MACRO cube to determine the N and C contents in poly-ethylenimine and amine-impregnated sorbents. Then the amine loading of amine-functioned adsorbents could be calculated. Before the N_2 physisorption and the elemental analysis test, samples were vacuum degassed at 60 °C overnight. The CO_2 adsorption and desorption rates were examined using NETZSCH STA 449 F5 (TGA) instrument.

3. Results and discussions

3.1. Difference between steam and nitrogen purge

The scheme of thermostatic concentration swing adsorption was shown in Fig. 2. Unlike conventional TSA, both adsorption and desorption process occurred at a constant temperature of 105 °C. In the adsorption process, CO_2 was adsorbed when simulated flue gas passed through the adsorption column. While during the adsorption process, CO_2 was desorbed when steam flowed through the adsorption column.

Fig. 3 represented the cyclic adsorption capacity of amine-modified adsorbent by TC-CSA. It can be found that there is no obvious loss of adsorption capacity within 20 cycles, indicating that the cycle process had a good cyclic stability. There was a decrease in adsorption capacity between the first and the second cycle because the adsorbent may not be able to desorb completely during the 30 min desorption time (the adsorbents before first cycle was desorbed overnight at 60 °C under vacuum), but the subsequent cyclic adsorption capacity maintained when the desorption conditions were fixed. In contrast to the results of most studies investigating the hydrothermal stability of amine-functionalized adsorbents, short-term, multiple exposures to steam did not lead to a decrease in CO_2 adsorption capacity, and this kind of exposure type was closer to the actual desorption scenarios. Hydrothermal stability of amine-modified adsorbents might not be a necessary research focus for

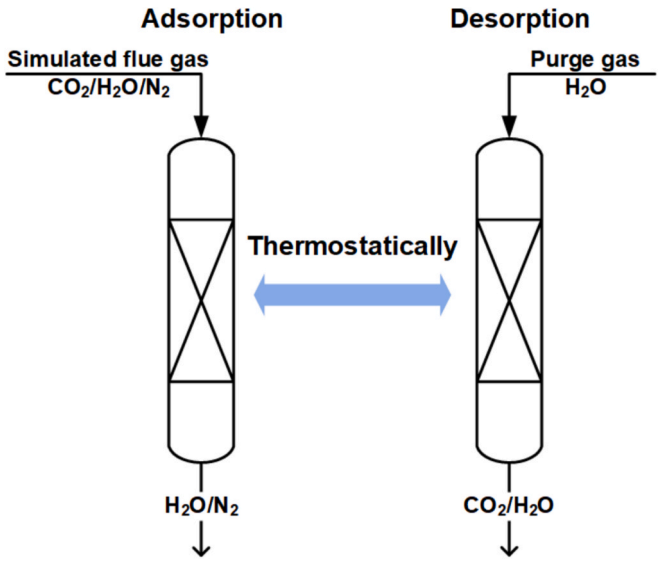

Fig. 2. The scheme of thermostatic concentration swing adsorption (TC-CSA).

certain supporting materials.

Although nitrogen purge resulted in remixing of CO_2 with nitrogen, here comparison with nitrogen purge indicated some specific effects of steam purge on CO_2 adsorption. The desorption time was fixed to 30 min and the nitrogen desorption flow rate was 62 SCCM, consistent with the steam flow rate after vaporization. Fig. 4(a) showed the comparison of adsorption breakthrough curves under nitrogen purge and steam purge. CO_2 adsorption capacity could be calculated by integrating over the upper left region of the breakthrough curve, as shown in Equation (1). The results showed that the CO_2 adsorption capacity under nitrogen purge was 1.32 ± 0.01 mmol/g, whereas the CO_2 adsorption capacity under nitrogen purge was 1.93 ± 0.02 mmol/g. Changing only the purge gas led to a change in the breakthrough curve. For steam purge conditions, the breakthrough time was 9 min, then C increased rapidly with adsorption time and approached to C_0. While for nitrogen purge, CO_2 could be detected at the initial moment, and then C/C_0 grew slowly with

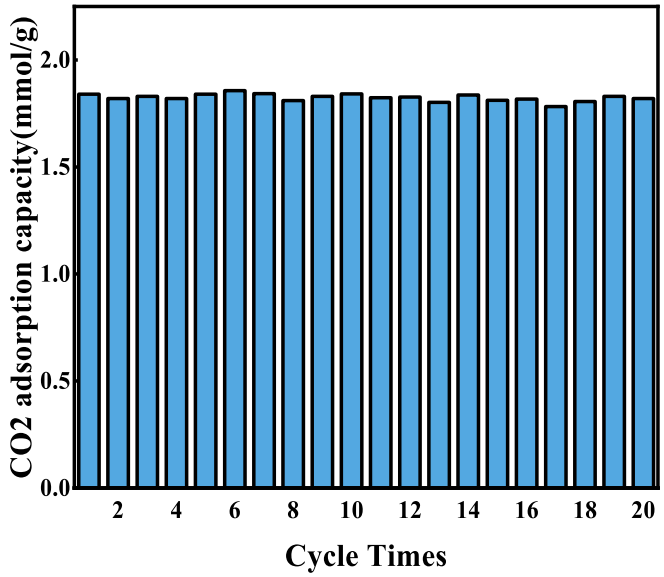

Fig. 3. CO_2 cyclic adsorption capacity of 50% PEI-γ-Al_2O_3 by TC-CSA.

time. The slope of the breakthrough curves stood for the adsorption kinetics [53]. Therefore, the adsorbent after steam purge had faster adsorption kinetics and higher CO_2 adsorption capacity compared to nitrogen purge.

Fig. 4(b) showed the temperature change of the adsorbent within a cycle. For desorption process of nitrogen purge, the temperature decreased to 103 °C at the initial moment because rapid CO_2 desorption took much heat. After 30 min, the inlet gas was switched to the simulated flue gas, the adsorbent temperature rose to 109 °C due to CO_2 adsorption. While for desorption process of steam purge, the temperature went up firstly, indicating steam could be adsorbed onto the amine-functionalized adsorbents. CO_2 was not desorbed at the initial moment of the steam purge as shown in Fig. 4(c), which was consistent with the former study [46,47]. The adsorbents adsorbed steam firstly, and CO_2 was desorbed only when the adsorbed steam reached a certain amount due to the adsorption sites occupancy and gas purging. The reason for the judgement that steam purge did not act only as purge effect was the huge difference in the desorption curves in Fig. 4(c). After a period of time, the outlet CO_2 flow of the nitrogen purge was significantly higher than that of the steam purge, which allowed for faster desorption. It was also worth noting that the temperature change during the steam purge is favorable to the CO_2 adsorption and desorption. High temperature promoted complete CO_2 desorption, while low temperature favored CO_2 adsorption.

3.2. The effect of adsorption temperature

Experiments at different adsorption temperatures (T_{ads}) were carried out to compare TC-CSA with the conventional TSA process. Fixed desorption temperature of 105 °C and steam purge for 30 min. Fig. 5(a) showed breakthrough curves at different adsorption temperatures. The breakthrough time gradually increased as the adsorption temperature decreased, while the slopes of the post-breakthrough CO_2 concentrations were indistinguishable, implying that there was no significant difference in the adsorption kinetics. The adsorption capacities were 3.53 ± 0.11 mmol/g, 2.82 ± 0.11 mmol/g and 1.93 ± 0.02 mmol/g at adsorption temperatures of 55 °C, 80 °C and 105 °C, respectively. The adsorption capacity decreased with increasing adsorption temperature in the range of 55–105 °C.

Fig. 5(b) showed the temperature variation within a cycle at different adsorption temperatures, where the small short lines in the corresponding colors represented the demarcation of the different processes

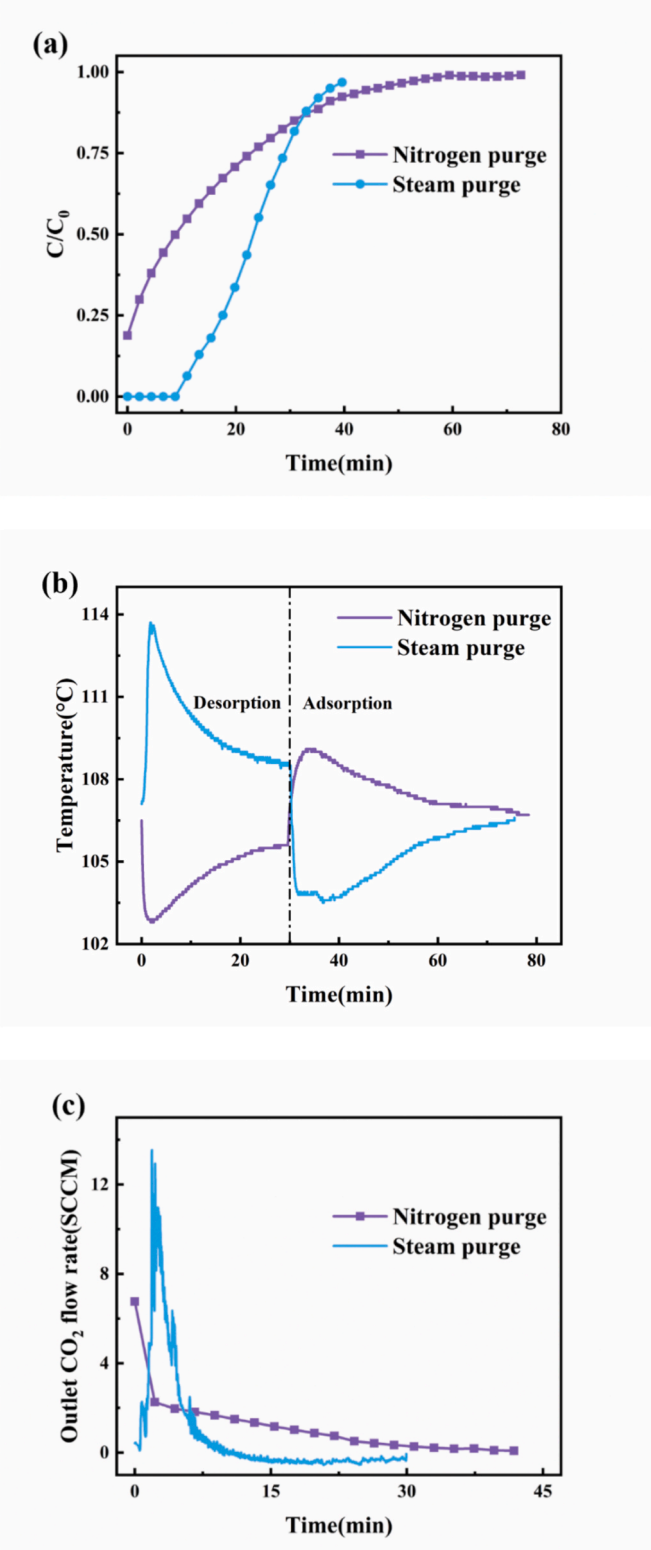

Fig. 4. (a) Breakthrough curves, (b) Temperature variety of adsorbent, (c) outlet CO_2 flow, under steam and nitrogen purge conditions.

in a cycle. There were only two processes at T_{ads} = 105 °C. For T_{ads} = 55 °C and 80 °C, i.e. conventional TSA process, one cycle included five processes in the order in Fig. 5(b): Heating process, steam purging process, nitrogen purge process (To remove steam from the system, otherwise direct cooling would result in water immersion of the adsorbent which would significantly reduce the adsorption capacity, and this

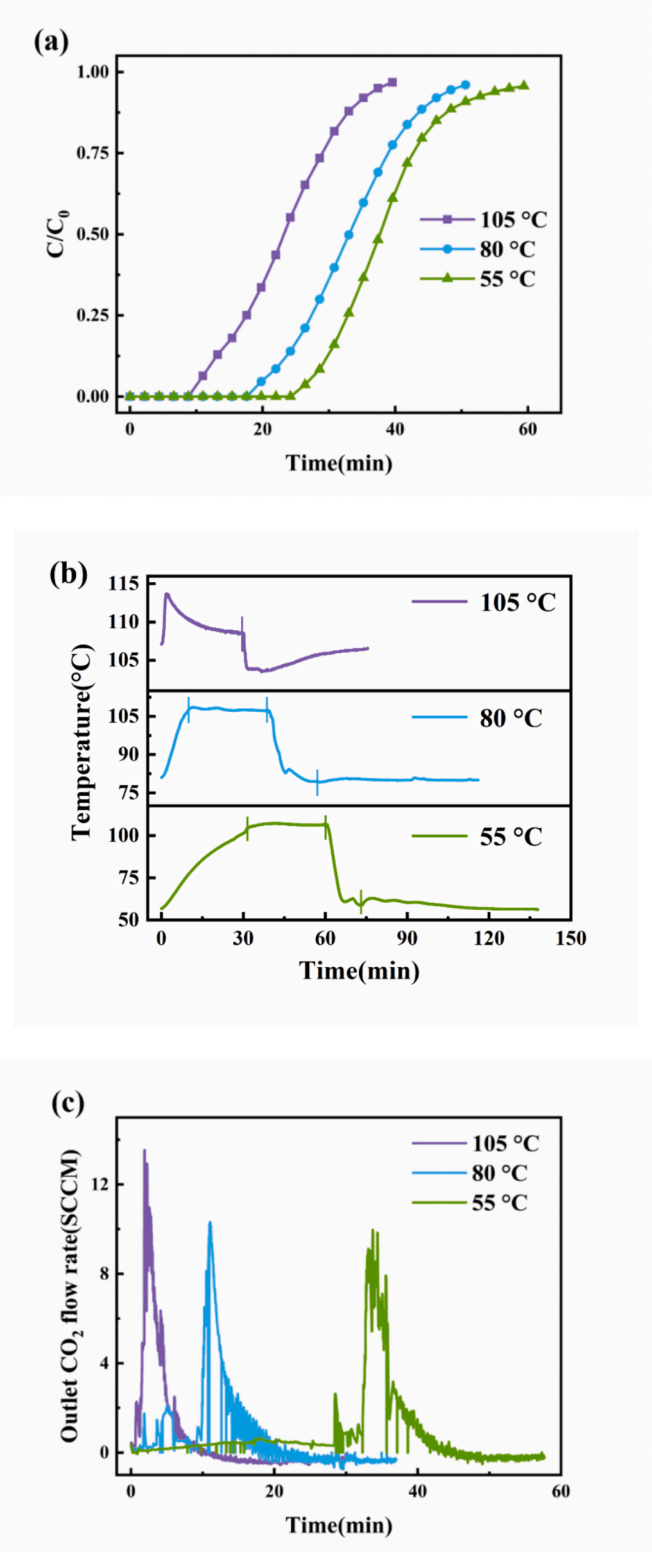

Fig. 5. (a) Breakthrough curves, (b) Temperature variety of adsorbent, (c) outlet CO_2 flow, at different adsorption temperatures.

process was not shown in the figure as the process took only 30 s), cooling process and adsorption process. The adsorbent temperature increased during the steam purging process, indicating that the exothermic effect of steam adsorption exceeded the endothermic effect of CO_2 adsorption. The peak of the adsorbent temperature of $T_{ads} = 55$ °C and 80 °C was lower than that of $T_{ads} = 105$ °C because less water was adsorbed during the steam purging process. When the water vapor content in the simulated flue gas was fixed, the lower adsorption temperature corresponded to the higher relative humidity, and the moisture adsorption capacity of the amine-functionalized adsorbents was positively correlated with the relative humidity [54,55]. The Outlet CO_2 flow rate at 105 °C was the highest as shown in Fig. 5(c) because of the highest desorption temperature. The shorter duration of one cycle of the TC-CSA process due to the elimination of the warming and cooling process facilitated rapid adsorption, as will be emphasized in the subsequent sections.

Fig. 6 showed the thermogravimetric curves of the 50 % PEI-γ-Al_2O_3 at different temperatures with 100 SCCM 15 %CO_2/85 %N_2 for the first 20 min and 100 SCCM pure nitrogen for the last 20 min. The first 20 min represented the adsorption process and the last 20 min represented the desorption process at the same temperature. Before the adsorption experiment, adsorbents were degassed at 120 °C for 20 min. Different from the humid CO_2 adsorption experiments, CO_2 adsorption capacity without moisture increased firstly and then declined with the increase of the adsorption temperature. At 100 °C, CO_2 adsorption capacity reached the maximum. The phenomenon was consistent with [23,56], at high amine loading, there was an optimal temperature for solid amine adsorbents to achieve highest CO_2 adsorption capacity. High temperature improved CO_2 diffusion, thus more amines could react with CO_2, which was also reflected in the figure, at the temperatures of 110 and 120 °C, the CO_2 adsorption reached equilibrium during the experiment period. At low temperatures, the CO_2 adsorption capacity was still slowly increasing after 20 min·H_2O adsorption could also enhance the CO_2 diffusion [37]. Therefore, CO_2 adsorption capacity was high at low temperature in the presence of humidity.

As mentioned in the previous paragraph, the CO_2 adsorption of some amines in the 50 % PEI-γ-$Al_2O_3$was affected by CO_2 diffusion. Therefore, the common pseudo-first order kinetic model [57] as shown in Equation (2) might not be suitable to describe the adsorption kinetic here, which regarded the adsorption rate as a constant. A dual-kinetic model worked well here [58,59], which posited the existence of two distinct adsorption rates within the solid amine. The faster rate indicated the reaction of CO_2 with the surface amine, while the slower rate represented the reaction rate of CO_2 with deep-layer amines after diffusing through the surface amine layer. It was worth noting that, adsorption rate k here included the effect of adsorption capacity. The value could not only indicate the time required for reaching the adsorption capacity equilibrium, but also was a comprehensive parameter to reflect the time to achieve a certain CO_2 adsorption capacity. As shown in Fig. 7, the dual-kinetic model could fit the experimental curve more accurately compared to the pseudo-first order kinetic model. The fitting results at different temperatures were presented in Table 2.

$$q = q_e(1 - e^{-kt}) \tag{2}$$

$$q = q_e[\varphi(1 - e^{\frac{-k_1 t}{q_e}}) + (1 - \varphi)(1 - e^{\frac{-k_2 t}{q_e}})] \tag{3}$$

where q_e is the equilibrium CO_2 adsorption capacity, mmol/g, q is the CO_2 adsorption capacity at time t, mmol/g, k_1 is the fast rate constant and k_2 is the slow rate constant, mmol/(g•s), φ is the percentage of rapid adsorption rate stage.

As shown in Table 2, φ showed an upward trend as the adsorption temperature increased, indicating that more amines were not influenced by CO_2 diffusion at high temperatures. Consistent with CO_2 adsorption capacity, fast adsorption rate increased firstly and then declined as the adsorption temperature rose. At high temperatures, CO_2 desorption dominated, greatly inhibiting the adsorption rate. While slow adsorption rate rose with the growth of temperature, which also signified that the CO_2 diffusivity increased with increasing temperature. Pseudo-first order kinetic model was used to describe the CO_2 desorption. As shown in Fig. 6, the desorption rate was mere below 70 °C, so the desorption rate was not displayed here. The desorption rate increased

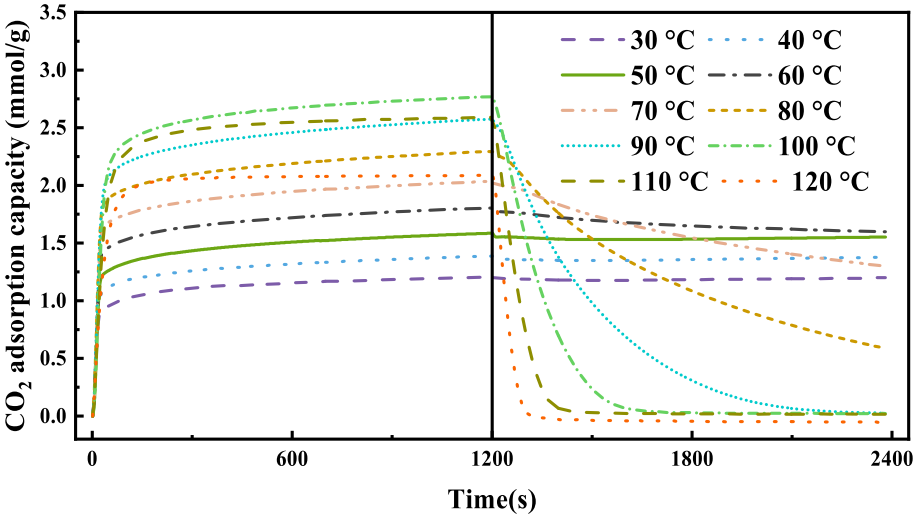

Fig. 6. Adsorption and desorption curves measured by TGA at different temperatures.

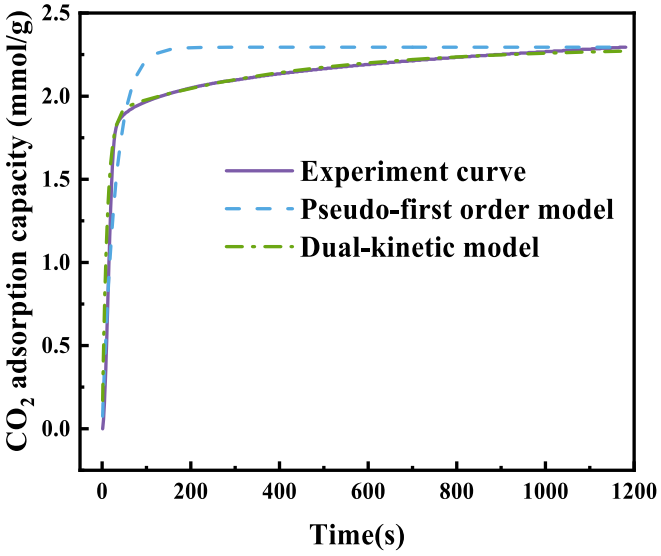

Fig. 7. Experimental curves and fitting results at 80 °C.

Table 2
CO_2 adsorption capacity and k of desorption and adsorption process at different adsorption temperatures.

T_{ad} (°C)	CO_2 adsorption capacity	Adsorption			Desorption
		φ	k_1	k_2	k
30	1.21	0.79	0.145	0.004	–
40	1.39	0.81	0.159	0.004	–
50	1.59	0.81	0.171	0.004	–
60	1.80	0.81	0.196	0.005	–
70	2.03	0.83	0.200	0.005	–
80	2.29	0.82	0.214	0.006	0.004
90	2.57	0.82	0.194	0.006	0.009
100	2.77	0.83	0.140	0.008	0.019
110	2.59	0.87	0.105	0.010	0.033
120	2.09	0.89	0.085	0.015	0.044

monotonically with the growth of temperature. For a given adsorbent, there is often an optimal temperature interval for a TC-CSA cycle, influenced by the adsorption and desorption kinetics and the adsorption thermodynamics. Notably, the results may be also useful for determining the optimal temperature for PSA and VSA. For 50 % PEI-γ-Al_2O_3, the appropriate temperature interval for TC-CSA should be 90–110 °C.

3.3. Economic analysis

Currently the most important factor limiting the large-scale industrial development of the carbon capture process is the high energy consumption, so the main focus here is on the possibilities of the TC-CSA process to reduce the energy consumption. The most commonly used energy consumption formula for solid adsorbents is shown in Equation (4) [60,61]. The regeneration energy is divided into three main parts: the sensible heat rising the adsorbents from adsorption temperature to desorption temperature, the desorption heat of CO_2 and H_2O.

$$Q = \frac{C_{p,s}\cdot(T_{Des} - T_{Ads})}{q_{CO_2}} + \Delta H_{CO_2} + \frac{q_{H_2O}}{q_{CO_2}}\Delta H_{H_2O} \quad (4)$$

where Q means the total energy consumed in a complete adsorption–desorption cycle, kJ/kg CO_2. q_{CO_2} is cyclic adsorption capacity, represents the amount of CO_2 that can be adsorbed by 1 g sorbent in one cycle, kg CO_2/kg adsorbent. $C_{p,s}$ is specific heat capacity at constant pressure, kJ/(kg•K). T_{des} is desorption temperature and T_{ads} is adsorption temperature, K. ΔH_{CO_2} and ΔH_{H_2O} is the adsorption heat of CO_2 and H_2O, kJ/kg. q_{H_2O} is H_2O adsorption capacity and q_{H_2O}/q_{CO_2} represents the selectivity of H_2O for CO_2.

To ensure the purity, it is necessary to purge pure CO_2 for desorption in real TSA. The CO_2 adsorption capacity in 100 % CO_2 environment was shown in Table 3. For 50 % PEI-γ-Al_2O_3, the adsorption capacity remained high at high temperatures. 170 °C was chosen as the desorption temperature to ensure sufficient cyclic adsorption capacity. Thermogravimetric curve in one cycle was shown in Fig. 8(a). Adsorbed CO_2 could not be fully desorbed at 170 °C under 100 % CO_2 environment, and the difference was equal to the CO_2 adsorption capacity under these conditions (0.51 mmol/g). As shown in Fig. 8(b), the adsorption capacity reduced by 17 % over 20 cycles. Therefore, the cyclic stability of 50 % PEI-γ-Al_2O_3 in TSA was poor. Based on the calculated parameters [61] and Equation (4), the theoretical energy consumption was calculated to be 3.55 MJ/kg.

For TC-CSA, the first term on the right side of Equation (4) is zero, while the second term is fixed for a fixed adsorbent, and the third term is

Table 3
CO_2 adsorption capacity of 50%PEI-γ-Al_2O_3 in 100% CO_2 environment.

Adsorption Temperature (°C)	150	160	170
CO2 adsorption capacity(mmol/g)	1.88	1.11	0.51

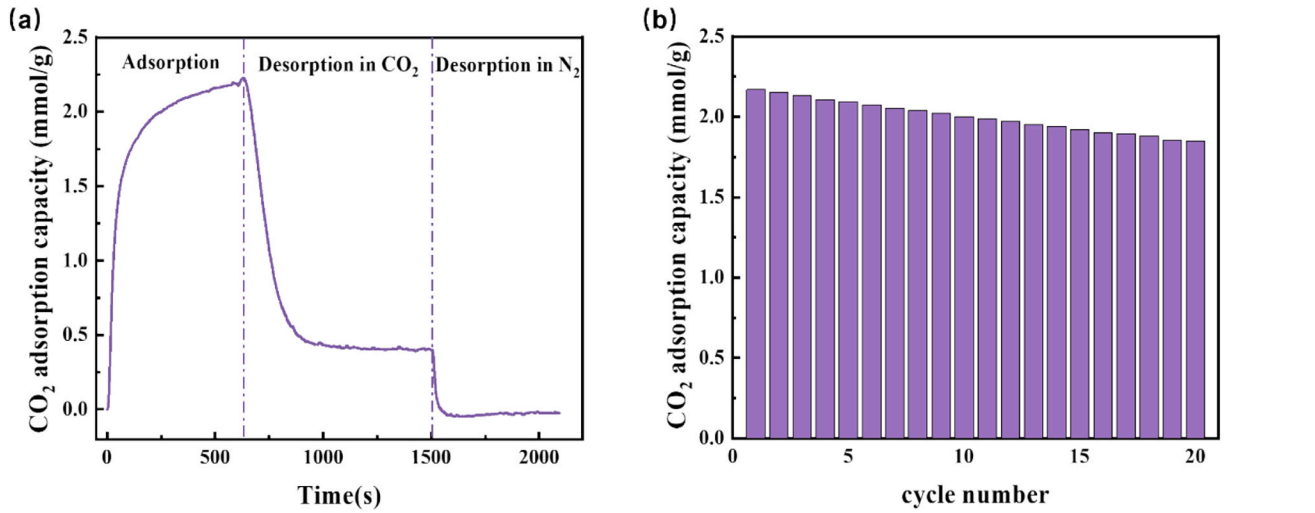

Fig. 8. (a) Thermogravimetric curve of 15 % CO_2 adsorption at 110 °C, pure CO_2 desorption at 170 °C and pure N_2 desorption at 170 °C (b) 20 cycles of CO_2 adsorption capacity in TSA.

also low because H_2O adsorption capacity is low at a high adsorption temperature. In summary, TC-CSA is able to reduce energy consumption compared to the conventional TSA process.

Considering that the temperature of flue gas from coal-fired power plants is 55 °C, sensible heat raising the flue gas to 105 °C may be required for TC-CSA. The sensible heat can be calculated by Equation (5), the detailed calculation parameters are shown in Table 4.

$$Q_{sen} = \sum x_i \Delta H_i \quad (5)$$

where x_i is the mass ratio of component i to CO_2 in the flue gas, ΔH_i is the enthalpy difference of component i between 55 °C and 105 °C, kJ/kg. The energy required to raise the temperature of flue gas containing 1 kg CO_2 was 273.89 kJ/kg CO_2. While the energy required to raise the temperature of solid adsorbent containing 1 kg CO_2 was 832.09 kJ/kg CO_2 as shown in Table 5. The energy consumption to raise the flue gas temperature is much lower than energy to raise the adsorbent temperature. In some scenarios, the flue gas temperature itself is near 105 °C, TC-CSA can be directly applied to carbon capture of these flue gas as well.

The energy consumption of TC-CSA is mainly the enthalpy of water vapor supplied to the adsorption bed, which has an extremely high latent heat of vaporization of 2258.4 kJ/kg. To reduce the consumption of water vapor, one strategy is to reduce the desorption time. According to the results in Fig. 6, the desorption rate was fast in the early stage of desorption. To utilize the property, the desorption capacity at decreasing desorption time was measured, as shown in Fig. 9. The two curves represented the ratio of the CO_2 desorption capacity at $T_{ads} = 55$ or 80 °C to the CO_2 desorption capacity at $T_{ads} = 105$ °C. All the desorption capacity declined with decreasing desorption time, representing an increase in the degree of incomplete desorption. Although shorter desorption duration reduced the CO_2 desorption capacity, the reduction in desorption capacity was much lower than the reduction in desorption time. Compared with nitrogen purge, steam purge favored rapid CO2 desorption, and a large CO_2 desorption capacity can be obtained in a short desorption time. The ratio of CO_2 desorption capacity at $T_{ads} = 55$ or 80 °C to the CO_2 desorption capacity at $T_{ads} = 105$ °C gradually decreased as the desorption time decreased, indicating CO_2 desorption capacity at $T_{ads} = 55$ or 80 °C decreased faster. At low adsorption temperatures, CO_2 bonded to some adsorption sites that are difficult to desorb, and these CO_2 could not desorb within a short desorption time. There was a lift at the end of the curve because some CO_2 desorbed during the heating process as shown in Fig. 5(c), and the effect became more prominent during the shorter desorption time.

Table 4
The sensible heat needed to raise the temperature of flue gas.

Component	C_i (%)	x_i	ΔH_i(kJ/kg)	Q_{sen} (kJ/kg CO_2)
CO_2	12.9	1	44.72	273.89
H_2O	13	0.412	94.14	
N_2	74.1	3.655	52.09	

Table 5
The sensible heat needed to raise the temperature of adsorbent.

$C_{p,s}$ (kJ/kg•K)	ΔT (K)	q_{CO_2}(g /g)	Q_{sen} (kJ/kg CO_2)
2.23	50	0.134	832.09

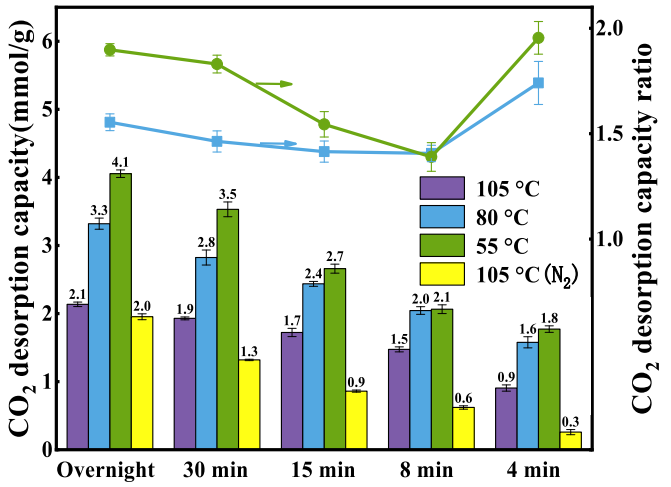

Fig. 9. CO_2 desorption capacity at different desorption time.

The mass of water vapor required to desorb 1 kg CO_2 can be calculated in Equation (6).

$$\alpha = m_{H_2O}/m_{CO_2} \quad (6)$$

α at different desorption time was shown in Fig. 10. As desorption time decreased, α gradually decreased. When the desorption duration was 4 min, the desorption of 1 kg CO_2 still required about 5 kg of water vapor, demanding a minimum latent heat consumption of 11.27 MJ,

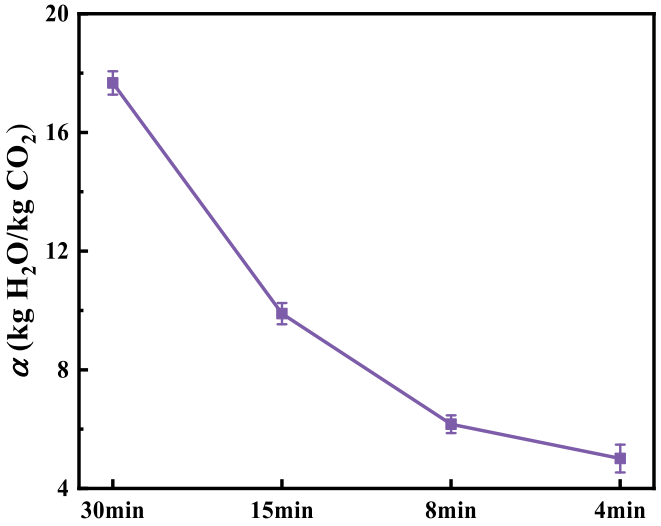

Fig. 10. Water vapor consumption at different desorption time.

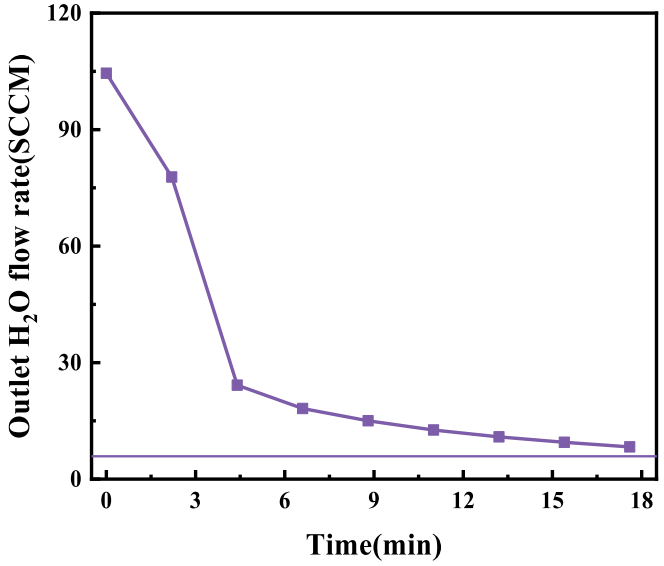

Fig. 12. The variety of water vapor flow rate with time during the adsorption process.

which is an impractical energy cost.

The enthalpy of water vapor can be recovered with a heat exchanger, as illustrated in Fig. 11. The mixture of desorbed CO_2 and water vapor enters into the heat exchanger and is cooled to 60 °C as a hot stream, causing most of the water vapor to condense and releases significant latent heat. Then the mixture enters into gas–liquid separator, liquid water passes through the heat exchanger as a cold stream and is heated and vaporized to water vapor again as purge gas. Additionally, during steam purge, some of the water vapor is adsorbed by adsorbents, which is desorbed again during adsorption. Fig. 12 illustrated the variation of water vapor flow during adsorption, where the horizontal line on the lower side indicated the water vapor flow rate contained in the simulated flue gas itself. The area between the two lines represents the water vapor desorption capacity. The large content of water vapor in the early stage of the adsorption process can likewise be used for heat transfer.

The proportion of reusable water vapor χ can be calculated by Equation (7) [62,63].

$$\chi = \delta_{ads}\theta\left(1-\frac{(1-y_{ads,H_2O})P_{T,sat}}{y_{ads,H_2O}(1-P_{T,sat})}\right)+(1-\delta_{ads})\left(1-\frac{(1-y_{des,H_2O})P_{T,sat}}{y_{des,H_2O}(1-P_{T,sat})}\right) \quad (7)$$

Here, the first term on the right indicates the proportion of water vapor that can be reused in the adsorption process, while the second term is that during desorption. δ_{ads} denotes the mass ratio of adsorbed water vapor to the total water vapor, θ means the mass ratio of utilized water vapor with highwater vapor content to the adsorbed water vapor, y denotes the water vapor content, and $P_{T,cold}$ represents the ratio of the saturated water vapor pressure to the ambient pressure at the temperature of cold flow.

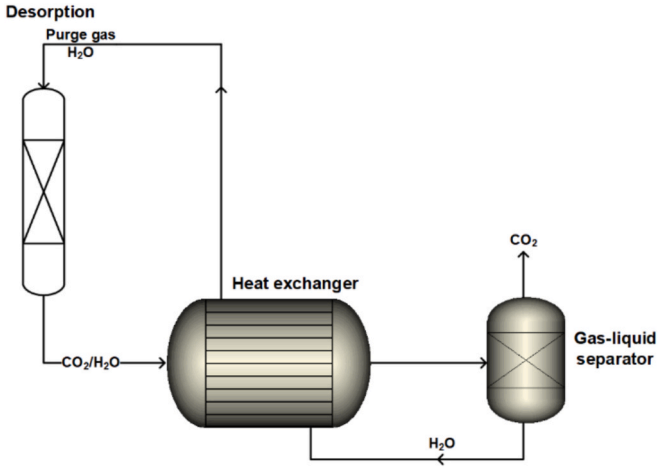

Fig. 11. The flowsheet of TC-CSA combined with steam heat exchange.

When the desorption time is 8 min, it was calculated that after heat exchange, about 87 % of the water vapor could be recycled as purge gas. Only an additional 0.79 kg of water vapor must be supplied for an energy requirement of 2049 kJ/kg, significantly lower than the energy consumption for conventional TSA. In addition, there is still a significant amount of waste heat in the system that is not recovered, such as the gas with low water vapor content at 105 °C during adsorption and the 60 °C CO_2 at the outlet of the gas–liquid separator.

It is worth noting that the energy analysis here is specific to the experimental conditions in this study, for TC-CSA, there are still optimization opportunities, such as the solid amine adsorbents, adsorption/desorption flow rates, adsorption bed heat transfer conditions, adsorption temperature, and so on. The system holds significant potential for further energy consumption reduction

Table 6 exhibited the comparison of TC-CSA with industrial benchmarks in terms of adsorption capacity, energy consumption, and regeneration rate. It can be found that TC-CSA have advantages in terms of energy consumption and regeneration rate.

Nevertheless, adsorption at 105 °C led to a decrease in the adsorption capacity as described in Fig. 5(a). And the duration of a cycle was shorter by eliminating the heating and cooling process. For rapid adsorption, a parameter, productivity W, was usually used to express the CO_2 adsorption capacity per unit time.

$$W = q_{CO_2}/t_{cycle} \quad (6)$$

Fig. 13 showed productivity W at different adsorption temperatures with desorption time. At T_{ads} = 105 °C, the reduction in desorption time had a significant effect on increasing productivity due to the short cycle duration time, so productivity increased rapidly at short desorption time. The productivity at T_{ads} = 105 °C was greater than at lower temperatures under all conditions, implying that TC-CSA favored rapid CO_2 capture. It is worth noting that the above results were obtained in the experimental conditions. There were extremely large CO_2 emissions of 8 t/min in a 600 MW coal-fired power plant, to reduce the scale of carbon capture devices, the solid adsorbents were required to be able to quick adsorption/desorption. It had been suggested that a full cycle of adsorption/desorption should be 15–30 min [42]. In such a short cycle time, heating and cooling a large amount of adsorbent was difficult, and

Table 6
Comparison of TC-CSA with industrial benchmarks in terms of adsorption capacity, energy consumption, and regeneration rate.

Technology	Material	CO_2 capacity (mmol/g)	Energy Consumption (MJ/kg CO_2)	regeneration rate	Reference
Amine solution + TSA	30 %MEA	2.85	4.0	34 % in 2 h	[64]
Biphasic solvents + TSA	3DT3G4H	2.3	2.4	70 % in 2 h	[24]
solid sorbents + TSA	Lewatit VP OC 1065	1.69	4.2	32 % in 5 min	[65]
Solid adsorbents + TSA	50 %PEI-γ-Al_2O_3	2.26	3.55	76 % in 5 min	This work
Solid adsorbents + TC-CSA + heat exchange	50 %PEI-γ-Al_2O_3	1.92	2.05	100 % in 5 min	This work

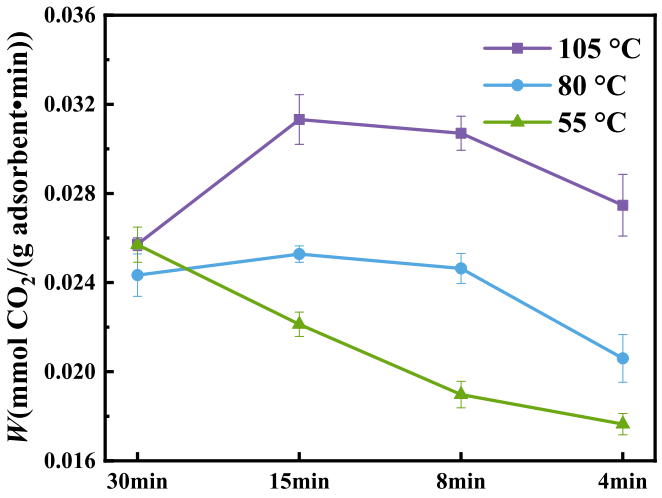

Fig. 13. Productivity *W* at different desorption time.

the long duration of heating and cooling process would contribute to the further decrease in productivity, consequently increasing the amount of adsorbent. Therefore, TC-CSA is definitely more suitable for carbon capture from flue gas of coal-fired power plants than the conventional TSA process.

4. Conclusion

In this paper, the adaptability of thermostatic concentration swing adsorption for amine-modified adsorbents was explored, a comparison was made between the use of steam purge and nitrogen purge, the effect of different adsorption temperatures on CO_2 adsorption was analyzed. Finally, the advantage of thermostatic concentration swing adsorption was verified in terms of the energy consumption and the productivity. The following conclusions were obtained:

Steam purge was more advantageous than nitrogen purge in adsorption capacity and adsorption/desorption kinetics. In addition to purging, steam could adsorb on the adsorbent as a replacement of CO_2, thus exhibiting the opposed temperature variations compared to nitrogen purge. The adsorption capacity increased with the decrease of adsorption temperature, and the adsorption capacities were 3.53 ± 0.11 mmol/g, 2.82 ± 0.11 mmol/g and 1.93 ± 0.02 mmol/g at the adsorption temperatures of 55, 80, and 105 °C, respectively. While for CO_2 adsorption without humidity, the adsorption capacity firstly increased and then declined with the growth of adsorption temperature. The presence of humidity improved the CO_2 diffusion. Consistent with CO_2 adsorption capacity, fast adsorption rate increased firstly and then declined as the adsorption temperature rose. The temperature interval of 90–110 °C contributed to fast adsorption and desorption for 50 % PEI-γ-Al_2O_3. Thermostatic concentration swing adsorption had a great potential for energy-saving by avoiding sensible heat energy compared to conventional TSA. Also, the cycle process presented advantages in productivity. Reducing the desorption time had a minimal effect on the CO_2 adsorption capacity at the adsorption temperature of 105 °C. Considering the extremely high CO_2 emissions from coal-fired power plants, Thermostatic concentration swing adsorption without heating and cooling time is a competitive alternative cycle process for amine-functionalized adsorbents.

CRediT authorship contribution statement

Shun Wang: Writing – review & editing, Writing – original draft, Methodology, Formal analysis. **Shujuan Wang:** Validation, Supervision. **Yuqun Zhuo:** Writing – review & editing, Supervision, Methodology, Formal analysis.

Declaration of competing interest

The authors declare that they have no known competing financial interests or personal relationships that could have appeared to influence the work reported in this paper.

Data availability

Data will be made available on request.

References

[1] Younas M, Rezakazemi M, Daud M, Wazir MB, Ahmad S, et al. Recent progress and remaining challenges in post-combustion CO2 capture using metal-organic frameworks (MOFs). Prog Energy Combust Sci 2020;80:100849. https://doi.org/10.1016/j.pecs.2020.100849.
[2] Daryayehsalameh B, Nabavi M, Vaferi B. Modeling of CO2 capture ability of [Bmim][BF4] ionic liquid using connectionist smart paradigms. Environ Technol Innov 2021;22:101484. https://doi.org/10.1016/j.eti.2021.101484.
[3] Szima S, Nazir SM, Cloete S, Amini S, Fogarasi S, et al. Gas switching reforming for flexible power and hydrogen production to balance variable renewables. Renew Sustain Energy Rev 2019;110:207–19. https://doi.org/10.1016/j.rser.2019.03.061.
[4] Carlson CJ, Albery GF, Merow C, Trisos CH, Zipfel CM, et al. Climate change increases cross-species viral transmission risk. Nature 2022. https://doi.org/10.1038/s41586-022-04788-w.
[5] CO_2 emissions in 2023. International Energy Agency, 2023. https://www.iea.org/reports/co2-emissions-in-2023.
[6] F Birol. World Energy Outlook 2023. 2023. https://www.iea.org/reports/world-energy-outlook-2023.
[7] S Dale. Statistical Review of World Energy. BP p.l.c., 2022. https://www.bp.com/en/global/corporate/energy-economics/statistical-review-of-world-energy.html.
[8] Raganati F, Ammendola P. CO2 Post-combustion capture: a critical review of current technologies and future directions. Energy Fuel 2024;38(15):13858–905. https://doi.org/10.1021/acs.energyfuels.4c02513.
[9] Raganati F, Miccio F, Iervolino G, Papa E, Ammendola P. Waste-derived tuff for CO2 capture: enhanced CO2 adsorption performances by cation-exchange tailoring. J Ind Eng Chem 2024;138:153–64. https://doi.org/10.1016/j.jiec.2024.03.049.
[10] Raganati F, Bellusci M, Leardi F, Varsano F, Ammendola P. CALF-20 obtained by mechanochemical synthesis for temperature swing adsorption CO2 capture: a thermodynamic and kinetic study. Chem Eng J 2025;506:159966. https://doi.org/10.1016/j.cej.2025.159966.
[11] Li Z, Feng S, Yang X, Lyu H, Wei S, et al. A review of biomass porous carbon for carbon dioxide adsorption from flue gas: physicochemical properties and performance. Fuel 2025;387:134318. https://doi.org/10.1016/j.fuel.2025.134318.
[12] Ye W, Tang Y, Liang X, Luo Q, Liang W, et al. Amine-impregnated as-synthesized silicas for CO2 capture: experimental study and mechanism analysis. Chem Eng Sci 2024;300:120614. https://doi.org/10.1016/j.ces.2024.120614.
[13] Pham TV, Hirano T, Cao KLA, Septiani EL, Tanabe E, et al. Facilitating gas accessibility via macropore engineering in amine-loaded silica particles for enhanced CO2 adsorption performance. Energy Fuel 2024;38(17):16743–55. https://doi.org/10.1021/acs.energyfuels.4c02937.

[14] Zheng S, Jiang Y, Jia S, Wu Y, Cui P. Effect of the presence of trace sulfur dioxide on piperazine-based amine absorbents for carbon dioxide capture. Chin J Chem Eng 2024. https://doi.org/10.1016/j.cjche.2024.05.003.
[15] Nie L, Mu Y, Jin J, Chen J, Mi J. Recent developments and consideration issues in solid adsorbents for CO2 capture from flue gas. Chin J Chem Eng 2018;26(11): 2303–17. https://doi.org/10.1016/j.cjche.2018.07.012.
[16] Chen Y, Lin G, Chen S. Preparation of a solid amine microspherical adsorbent with high CO2 adsorption capacity. Langmuir 2020;36(26):7715–23. https://doi.org/10.1021/acs.langmuir.9b03694.
[17] Chen Y, Zhang J, Liu H, Wang X, Chen S. A surfactant modified solid amine adsorbent to enhance CO2 adsorption performance. Colloids Surf A Physicochem Eng Asp 2023;677:132323. https://doi.org/10.1016/j.colsurfa.2023.132323.
[18] Darunte LA, Walton KS, Sholl DS, Jones CW. CO2 capture via adsorption in amine-functionalized sorbents. Curr Opin Chem Eng 2016;12:82–90. https://doi.org/10.1016/j.coche.2016.03.002.
[19] Wu J, Chen H, Lv S, Zhou Y. Kinetics and thermodynamics study on low energy synthesis of porous geopolymer based solid amine sorbent for efficient CO2 capture. J Environ Chem Eng 2024;12(1):111808. https://doi.org/10.1016/j.jece.2023.111808.
[20] Li X, Li R, Peng K, Zhao K, Bai M, et al. Amine-impregnated porous carbon–silica sheets derived from vermiculite with superior adsorption capability and cyclic stability for CO2 capture. Chem Eng J 2023;464:142662. https://doi.org/10.1016/j.cej.2023.142662.
[21] Zhang J, Guo S, Wang S, Tan X. Separation and capture of CO2 from ambient air using TEPA-functionalized PAN hollow fibers. Sep Purif Technol 2023;324: 124635. https://doi.org/10.1016/j.seppur.2023.124635.
[22] N F Mohamad, N H Abdul Rani, M S Md Zaini, N H Sabri, A N Mat Nor, et al. Synthesis and characterization of impregnated activated carbon coal bottom ash (AC-CBA) with Imidazole (Ims) and Tetraethylenepentamine (TEPA) for carbon capture. Materials Today: Proceedings 2023. DOI: https://doi.org/10.1016/j.matpr.2023.01.104.
[23] Lin L, Ju T, Han S, Meng F, Li J, et al. Comparison of characteristics and performance between PEI and DETA impregnated on SBA-15 for CO2 capture. Sep Purif Technol 2023;322:124346. https://doi.org/10.1016/j.seppur.2023.124346.
[24] Cui Y, Guo D, Chen X, Zhou Y, Wang Z, et al. The impact of directly introducing aromatic nitrogen heterocycles on the performance of CO2 capture by diethylenetriamine/diethylene glycol dimethyl ether biphasic solvents: experimental and theoretical analysis. Chem Eng J 2025;163625. https://doi.org/10.1016/j.cej.2025.163625.
[25] Jahandar Lashaki M, Sayari A. CO2 capture using triamine-grafted SBA-15: the impact of the support pore structure. Chem Eng J 2018;334:1260–9. https://doi.org/10.1016/j.cej.2017.10.103.
[26] Hicks JC, Drese JH, Fauth DJ, Gray ML, Qi G, et al. Designing adsorbents for CO2 capture from flue gas-hyperbranched aminosilicas capable of capturing CO2 reversibly. J Am Chem Soc 2008;130(10):2902–3. https://doi.org/10.1021/ja077795v.
[27] Anyanwu J-T, Wang Y, Yang RT. Tunable amine loading of amine grafted mesoporous silica grafted at room temperature: applications for CO2 capture. Chem Eng Sci 2022;254:117626. https://doi.org/10.1016/j.ces.2022.117626.
[28] N H Sabri, N H A Rani, N F Mohamad, N a S Mohd Muhsen, M S Md Zaini. Simulation of CO2 capture for amine impregnated activated carbon - palm kernel shell (AC-PKS) adsorbent in pressure swing adsorption (PSA) using Aspen Adsorption. Materials Today: Proceedings 2023. DOI: https://doi.org/10.1016/j.matpr.2022.12.206.
[29] Krishnamurthy S, Lind A, Bouzga A, Pierchala J, Blom R. Post combustion carbon capture with supported amine sorbents: from adsorbent characterization to process simulation and optimization. Chem Eng J 2021;406:127121. https://doi.org/10.1016/j.cej.2020.127121.
[30] Yancy-Caballero D, Hughes R, Zamarripa MA, Omell B, Matuszewski M, et al. Isotherm modeling and techno-economic analysis of a TSA moving bed process using a tetraamine-appended MOF for NGCC applications. Int J Greenhouse Gas Control 2023;128:103957. https://doi.org/10.1016/j.ijggc.2023.103957.
[31] Vannak H, Osaka Y, Tsujiguchi T, Kodama A. The efficacy of carbon molecular sieve and solid amine for CO2 separation from a simulated wet flue gas by an internally heated/cooled temperature swing adsorption process. Appl Therm Eng 2024;239:122145. https://doi.org/10.1016/j.applthermaleng.2023.122145.
[32] Chen X, Wang J, Du T, Liu L, Kevin Li G. Process design and adsorbent screening of VSA and exchanger type VTSA for flue gas CO2 capture. Sep Purif Technol 2024; 348:127641. https://doi.org/10.1016/j.seppur.2024.127641.
[33] Chen X, Wang J, Du T, Liu L, Wang Y, et al. Post-combustion CO2 capture using exchanger type vacuum temperature swing adsorption: cycle design and performance analysis. Energ Conver Manage 2023;296:117625. https://doi.org/10.1016/j.enconman.2023.117625.
[34] Chatziasteriou CC, Georgiadis MC, Kikkinides ES. Modeling and optimization of an integrated membrane – P/VSA separation process for CO2 removal from coal plant flue gas. Chem Eng Res Des 2024;207:49–64. https://doi.org/10.1016/j.cherd.2024.05.016.
[35] Nokpho P, Amornsin P-O, Boonmatoon P, Wang X, Chalermsinsuwan B. Evaluating regeneration performance of amine functionalized solid sorbents for direct air CO2 capture using microwave. Mater Today Sustainability 2024;26:100728. https://doi.org/10.1016/j.mtsust.2024.100728.
[36] Verougstraete B, Schoukens M, Sutens B, Vanden Haute N, De Vos Y, et al. Electrical swing adsorption on 3D-printed activated carbon monoliths for CO2 capture from biogas. Sep Purif Technol 2022;299:121660. https://doi.org/10.1016/j.seppur.2022.121660.
[37] Mcdonald TM, Mason JA, Kong XQ, Bloch ED, Gygi D, et al. Cooperative insertion of CO2 in diamine-appended metal-organic frameworks. Nature 2015;519(7543): 303-+. https://doi.org/10.1038/nature14327.
[38] Choi W, Min K, Kim C, Ko YS, Jeon JW, et al. Epoxide-functionalization of polyethyleneimine for synthesis of stable carbon dioxide adsorbent in temperature swing adsorption. Nat Commun 2016;7:12640. https://doi.org/10.1038/ncomms12640.
[39] Xu C, Zhang Y, Peng Y-L, Yang T, Liu Z, et al. Degradation characteristics and utilization strategies of a covalent bonded resin-based solid amine during capturing CO2 from flue gas. Sep Purif Technol 2024;331:125621. https://doi.org/10.1016/j.seppur.2023.125621.
[40] Hu S, Miao Y, Guo Y, Wu H, Miao Y. Amine-impregnated cellulose aerogels prepared from old corrugated containers: microstructure characterization and CO2 capture performance. Chem Eng Sci 2025;302:120737. https://doi.org/10.1016/j.ces.2024.120737.
[41] Sun X, Zhu L, Wang P, Zhao W, Chen X. CO2 removal from natural gas by moisture swing adsorption. Chem Eng Res Des 2021;176:162–8. https://doi.org/10.1016/j.cherd.2021.09.033.
[42] Verougstraete B, Martín-Calvo A, Van Der Perre S, Baron G, Finsy V, et al. A new honeycomb carbon monolith for CO2 capture by rapid temperature swing adsorption using steam regeneration. Chem Eng J 2020;383:123075. https://doi.org/10.1016/j.cej.2019.123075.
[43] Li W, Choi S, Drese JH, Hornbostel M, Krishnan G, et al. Steam-stripping for regeneration of supported amine-based CO2 adsorbents. ChemSusChem 2010;3(8): 899–903. https://doi.org/10.1002/cssc.201000131.
[44] Jahandar Lashaki M, Ziaei-Azad H, Sayari A. Unprecedented improvement of the hydrothermal stability of amine-grafted MCM-41 silica for CO2 capture via aluminum incorporation. Chem Eng J 2022;450:138393. https://doi.org/10.1016/j.cej.2022.138393.
[45] Fayaz M, Sayari A. Long-term effect of steam exposure on CO2 capture performance of amine-grafted silica. ACS Appl Mater Interfaces 2017;9(50): 43747–54. https://doi.org/10.1021/acsami.7b15463.
[46] Sandhu NK, Pudasainee D, Sarkar P, Gupta R. Steam regeneration of polyethylenimine-impregnated silica sorbent for postcombustion CO2 capture: a multicyclic study. Ind Eng Chem Res 2016;55(7):2210–20. https://doi.org/10.1021/acs.iecr.5b04741.
[47] Hammache S, Hoffman JS, Gray ML, Fauth DJ, Howard BH, et al. comprehensive study of the impact of steam on polyethyleneimine on silica for CO2 capture. Energy Fuel 2013;27(11):6899–905. https://doi.org/10.1021/ef401562w.
[48] Min K, Choi W, Choi M. Macroporous silica with thick framework for steam-stable and high-performance poly(ethyleneimine)/silica CO2 adsorbent. ChemSusChem 2017;10(11):2518–26. https://doi.org/10.1002/cssc.201700398.
[49] Chaikittisilp W, Kim H-J, Jones CW. Mesoporous alumina-supported amines as potential steam-stable adsorbents for capturing CO2 from simulated flue gas and ambient air. Energy Fuel 2011;25(11):5528–37. https://doi.org/10.1021/ef201224v.
[50] Fujiki J, Chowdhury FA, Yamada H, Yogo K. Highly efficient post-combustion CO2 capture by low-temperature steam-aided vacuum swing adsorption using a novel polyamine-based solid sorbent. Chem Eng J 2017;307:273–82. https://doi.org/10.1016/j.cej.2016.08.071.
[51] Yang M, Wang S, Xu L. Hydrophobic functionalized amine-impregnated resin for CO2 capture in humid air. Sep Purif Technol 2023;315:123606. https://doi.org/10.1016/j.seppur.2023.123606.
[52] Liu F, Kuang Y, Wang S, Chen S, Fu W. Preparation and characterization of molecularly imprinted solid amine adsorbent for CO2 adsorption. New J Chem 2018;42(12):10016–23. https://doi.org/10.1039/C8NJ00686E.
[53] Fu D, Park Y, Davis ME. Zinc containing small-pore zeolites for capture of low concentration carbon dioxide. Angew Chem Int Ed 2022;61(5):e202112916. https://doi.org/10.1002/anie.202112916.
[54] Veneman R, Frigka N, Zhao W, Li Z, Kersten S, et al. Adsorption of H2O and CO2 on supported amine sorbents. Int J Greenhouse Gas Control 2015;41:268–75. https://doi.org/10.1016/j.ijggc.2015.07.014.
[55] Jung W, Lee KS. Isotherm and kinetics modeling of simultaneous CO2 and H2O adsorption on an amine-functionalized solid sorbent. J Nat Gas Sci Eng 2020;84: 103489. https://doi.org/10.1016/j.jngse.2020.103489.
[56] Zhu S, Zhao B, Su Y. Multiple-amine functionalized γ–Al2O3 for post-combustion CO2 capture: performance, mechanism, and kinetics. Fuel 2025;380:133186. https://doi.org/10.1016/j.fuel.2024.133186.
[57] Serna-Guerrero R, Sayari A. Modeling adsorption of CO2 on amine-functionalized mesoporous silica. 2: kinetics and breakthrough curves. Chem Eng J 2010;161(1): 182–90. https://doi.org/10.1016/j.cej.2010.04.042.
[58] Ohs B, Ködel M, Wessling M. Adsorption of carbon dioxide on solid amine-functionalized sorbents: a dual kinetic model. Sep Purif Technol 2018;204:13–20. https://doi.org/10.1016/j.seppur.2018.04.009.
[59] Bollini P, Brunelli NA, Didas SA, Jones CW. Dynamics of CO2 adsorption on amine adsorbents. 2. insights into adsorbent design. Ind Eng Chem Res 2012;51(46): 15153–62. https://doi.org/10.1021/ie3017913.
[60] Xu C, Zhang Y, Yang T, Jia X, Qiu F, et al. Adsorption mechanisms and regeneration heat analysis of a solid amine sorbent during CO2 capture in wet flue gas. Energy 2023;284:129379. https://doi.org/10.1016/j.energy.2023.129379.
[61] Zhang W, Liu H, Sun Y, Cakstins J, Sun C, et al. Parametric study on the regeneration heat requirement of an amine-based solid adsorbent process for post-combustion carbon capture. Appl Energy 2016;168:394–405. https://doi.org/10.1016/j.apenergy.2016.01.049.

[62] Liu W, Huang Y, Zhang XJ, Fang MX, Liu X, et al. Steam-assisted temperature swing adsorption for carbon capture integrated with heat pump. Case Stud Therm Eng 2023;49:103233. https://doi.org/10.1016/j.csite.2023.103233.
[63] Zhang M, Ge B, Gan Z, Liu S, Li S, et al. Integrated power to methanol processes with steam-assisted direct air capture. Energ Conver Manage 2025;326:119505. https://doi.org/10.1016/j.enconman.2025.119505.
[64] Li G, Shen X, Jiao X, Xie F, Hua J, et al. Novel tri-solvent amines absorption for flue gas CO2 capture: efficient absorption and regeneration with low energy consumption. Chem Eng J 2024;493:152699. https://doi.org/10.1016/j.cej.2024.152699.
[65] Sutanto S, Dijkstra JW, Pieterse J a Z, Boon J, Hauwert P, et al. CO2 removal from biogas with supported amine sorbents: first technical evaluation based on experimental data. Sep Purif Technol 2017;184:12–25. https://doi.org/10.1016/j.seppur.2017.04.030.